# Determinations of the Slope of the Chao Phraya Riverbank and Manning's Roughness Coefficient Utilizing Precise Point Positioning (PPP) Measurement Technique

**Thammaboribal, P.,[1*] Tripathi, N. K.,[1] Nakamura, S.[2] and Lipiloet, S.[3]**
[1]Asian Institute of Technology, School of Engineering and Technology, P.O. Box 4, Klong Luang, Pathumthani 12120, Thailand, E-mail: prapasgnss@gmail.com
[2]International Relations and Research Department Japan Aerospace Exploration Agency (JAXA), Japan
[3]Department of Civil Engineering, Faculty of Engineering, Rajamangala University of Technology Thanyaburi, Pathumthani 12120, Thailand
**Corresponding Author*

**DOI: https://doi.org/10.52939/ijg.v21i2.3953**

**Abstract**
*Flooding in Thailand, particularly in the Chao Phraya River basin, is a recurrent challenge exacerbated by seasonal monsoons. The catastrophic 2011 floods highlighted the urgent need for accurate flood prediction and management strategies. This study aimed to enhance flood modeling through precise determination of riverbank slopes and Manning's roughness coefficients using Global Navigation Satellite Systems (GNSS) and Precise Point Positioning (PPP) techniques. Elevation data were collected along the riverbanks from Ayutthaya to Bangkok using various GNSS positioning methods, with CSRS-PPP identified as the most reliable technique for height difference measurements. The study determined the river's slope to be approximately 0.00003, translating to a gradient of 1:33,333. Manning's roughness coefficients were calculated using observed discharge data and were found to range between 0.035 and 0.045 across different river stations. The derived roughness coefficients were validated against actual discharge measurements, revealing seasonal variations in flow resistance. The study further established empirical relationships between river depth, cross-sectional area, hydraulic radius, and discharge, enabling more accurate hydrological modeling. The results contribute to improved flood prediction and mitigation strategies by offering a reliable methodology for terrain elevation assessment and flow rate estimation in flood-prone regions.*

**Keywords:** Chao Phraya river, Discharge, Flow velocity, GNSS, PPP, Slope

## 1. Introduction

Flooding is a recurring disaster in Thailand, frequently exacerbated by the seasonal southwest monsoon, which occurs between May and November. This rainy season leads to significant flood events, often causing extensive damage throughout the country. In 2011, Thailand experienced an extraordinary event referred to as the "mega flood," which affected 65 out of the 77 provinces [1]. The flooding began in late October, persisted through the central and northern regions, and continued into January 2012, primarily impacting the Chao Phraya River basin [2].

The 2011 flooding caused widespread devastation, with over 800 deaths and more than 13.6 million people affected [3]. The industrial sector was severely impacted, particularly in large industrial estates that had never previously experienced flooding. This event revealed a critical gap in flood management: the lack of timely and accurate flood data, including flow rates, runoff volumes, and water depths [4]. As a result, people were ill-prepared to protect their properties, and the damage was far more extensive than expected. This highlights the crucial role that reliable flood information plays in disaster preparedness and mitigation planning [5]. The 2011 flood serves as a stark reminder of the need for advanced tools and methodologies to predict flooding events and mitigate their impacts. Accurate flood modeling, informed by up-to-date data on topography, flow rates, and terrain characteristics, is essential to improving flood response strategies and enhancing resilience in flood-prone regions [6][7] and [8].

Flood dynamics are influenced by several factors, with water flow rates primarily determined by the slope of the terrain and the roughness of the water channel [9] and [10]. Traditionally, slope calculations rely on differential leveling techniques, which involve the use of leveling instruments like the "level and rod". While effective, this method is time-consuming and expensive [11], particularly for large regions such as the Chao Phraya River basin in central Thailand.

Recent advancements in Global Navigation Satellite Systems (GNSS) have provided an alternative method for determining terrain elevation [12][13] and [14]. GNSS-derived "ellipsoid heights" can be converted into orthometric heights through Earth gravitational models (EGM), allowing for efficient topographic mapping of large areas [11]. Once terrain heights are established, the slope of the area can be calculated. Additionally, the water discharge can be modeled using Manning's equation, which considers the slope and cross-sectional area of the water flow, enabling the prediction of water travel time to specific areas [15] and [16]. This study aims to enhance flood modeling capabilities for the Chao Phraya River basin through the following objectives: (1) To measure the terrain elevation along the riverbanks from Ayutthaya to Bangkok using various GNSS techniques (single positioning, static positioning, and Precise Point Positioning (PPP)) and determine the optimal technique for data collection. (2) To compute the slope of the Chao Phraya River basin. (3) To back-calculate Manning's roughness coefficient (n-value) from cross-sectional parameters and the slope of the terrain. (4) To compute the flow rate of the Chao Phraya River using Manning's equation for open channel flow. And (5) to compare the computed discharge values with observed data from the Royal Irrigation Department of Thailand.

By achieving these objectives, the study seeks to improve flood prediction and management in the Chao Phraya River basin, contributing to better preparedness for future flood events.

## 2. Theoretical Backgrounds

### *2.1 Study Area*

The Chao Phraya River is a significant watercourse in Thailand, flowing entirely within the country and covering an approximate area of 160,000 km² [17]. The river traverses the central region of Thailand, which is characterized by a low alluvial plain. The Chao Phraya River originates at the confluence of the Ping and Nan rivers in Pak Nam Pho, located in Nakhon Sawan province [18], as illustrated in Figure 1. From this point, the river flows southward for 375 kilometers [19], passing through the central plain of Bangkok, the capital of Thailand, before draining into the Gulf of Thailand, which is part of both the Pacific Ocean and the South China Sea.

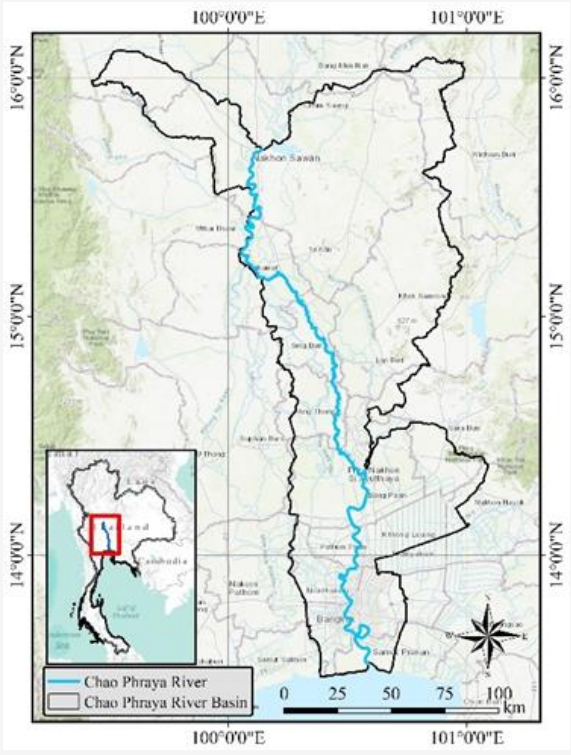


**Figure 1:** The Chao Phraya River, Basin

The river's approximate geographic coordinates are 13.58°N-15.67°N, 100.10°E -101.00°E [20]. The region experiences a wet monsoon climate, with annual rainfall exceeding 1,400 millimeters [21]. The rainy season lasts from May to October, supplemented by occasional storm depressions originating in the Pacific Ocean. The annual average temperatures in the area is approximately 27°C, with the maximum, temperature of 40°C in April [22], except in higher altitude regions. The basin itself is classified as a tropical rainforest, supporting a high level of biodiversity. The landscape surrounding the Chao Phraya River is a flat, expansive, and well-watered plain that is continuously replenished with soil and sediment carried by the river. In the northern part of the river basin, elevations exceed 20 meters, while the lower reaches of the river feature flat terrain, with an average elevation of approximately 2 meters above mean sea level. The region is composed of alluvial plains that support highly productive agricultural activities. Annual precipitation within the Chao Phraya River basin ranges from a minimum of 1,000 mm in the western regions to about 1,400 mm in the headwaters and up to 2,000 mm in the eastern Chao Phraya delta [23].

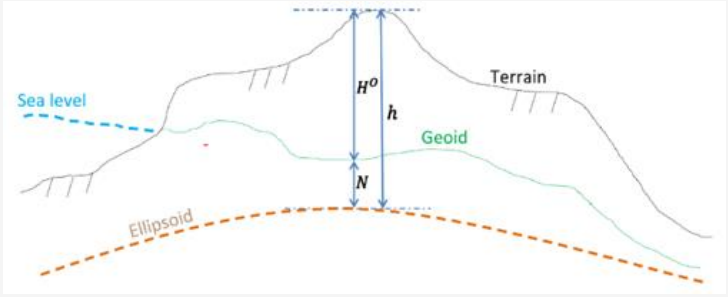


**Figure 2**: Ellipsoid height and orthometric height [25]

These precipitation values vary annually, contributing to both droughts and floods. Approximately 85% of the annual runoff occurs between July and December, with relatively low natural flows from January to June. The average annual discharge of the river is approximately 883 cubic meters per second (cms) [24]. The hydrological cycle of the Chao Phraya River begins in April, when discharge levels typically reach their minimum. From May to August, discharge gradually increases, with a more rapid rise observed between August and October. Discharge levels then decrease quickly in November and December, before slowing again until the next minimum flow period in April. During the January to April period, discharge typically ranges from 50 to 200 cms. The depth of the river varies between 5 and 20 meters, while its width spans from 200 to 1,200 meters [20].

*2.2 Ellipsoid Height*

Ellipsoid height is defined as the vertical distance above the reference ellipsoid, which is a mathematical model used to approximate the Earth's shape. In contrast, orthometric height refers to the vertical distance above the geoid, an imaginary surface that approximates mean sea level (MSL) and is influenced by Earth's gravity field (Figure 2). The relationship between ellipsoid height ($h$) and orthometric height ($H^0$) can be expressed by Equation 1.

$$h \approx H^0 + N$$

Equation 1

The ellipsoid height ($h$) refers to the elevation above the reference ellipsoid, which serves as an approximation of the Earth's surface, whereas orthometric height is measured relative to an imaginary surface called the geoid. The geoid, determined by the Earth's gravitational field, is commonly approximated by the mean sea level (MSL). The signed difference between the ellipsoid and geoid surfaces is known as the geoid undulation ($N$), which arises because the direction of the plumb line (the normal to the geoid) differs from the normal to the ellipsoid [25]. Geoid undulation values are computed by applying corrected values that convert pseudo-height anomalies, calculated at a point on the ellipsoid, into corresponding geoid undulation values [26]. The Earth Gravitational Model (EGM), developed and published by the National Geospatial-Intelligence Agency (NGA), is commonly employed for determining geoid undulation. The Office of Geomatics at NGA is responsible for the collection, processing, and evaluation of gravity data, including free-air and Bouguer gravity anomalies [27]. Gravimetric quantities such as mean gravity anomalies, geoid heights, and gravity disturbances are derived from the collected data. The EGM models published by NGA include EGM84, EGM96, and EGM2008, with the most recent version, EGM2008, being publicly available. EGM2008 is defined up to spherical harmonic degree and order 2159, with additional coefficients extending to degree 2190 and order 2159 [28]. Model coefficients can be accessed online at https://earth-info.nga.mil/. Geoid height can be computed online via the tool at https://earth-info.nga.mil/index.php?dir=wgs84&action=egm96-geoid-calc, and https://geographiclib.sourceforge.io/cgi-bin/GeoidEval where users input the receiver's position to automatically calculate the geoid heights for various EGM models.

*2.3 Precise Point Positioning*

GNSS receivers operating in favorable weather conditions with good satellite availability can achieve coordinates with horizontal accuracy of approximately 3–5 meters and vertical accuracy of 6–10 meters, within a 95% confidence interval [29][30] and [31]. The main sources of error in GNSS coordinates include atmospheric delays (ionospheric and tropospheric), satellite clock corrections, satellite geometry, and site-dependent effects such as multipath interference and measurement noise [32][33] and [34]. Physical obstructions that weaken satellite geometry can block satellite signals, resulting in degraded position accuracy [35].

Precise Point Positioning (PPP) is a technique that models or removes errors in the GNSS system to achieve high positioning accuracy using only a single GNSS receiver [36]. PPP accuracy primarily depends on corrections to satellite orbits and satellite clocks. This method can achieve decimeter-level positioning or better without requiring a base station [37]. The PPP solution requires a convergence period to achieve decimeter-level accuracy, allowing the resolution of local biases such as multipath effects, satellite geometry, and atmospheric conditions. The convergence time is influenced by the quality of the corrections and their application in the receiver. Under optimal conditions, PPP can achieve accuracy levels as precise as three centimeters [11]. When processing IGS orbits, Earth orientation parameters, and satellite clock corrections, various products are freely available at: https://cddis.nasa.gov/Data_and_Derived_Products/GNSS/orbit_and_clock_products.html.

*2.4 Manning's Roughness Coefficient*

The roughness coefficient in open channel flow is a numerical value that quantifies the resistance to flow caused by the roughness of the channel bed and sides. It is used in hydraulic engineering to estimate frictional losses in flowing water and is a key parameter in Manning's equation, which is commonly applied to calculate flow velocity and discharge in open channels, as shown in Equation 2 [38].

$$Q = \frac{1}{n} A R^{2/3} S^{1/2}$$

Equation 2

Where: $Q$ is discharge, $n$ is Manning's roughness coefficient, $A$ is cross-sectional area of flow, $R$ is hydraulic radius (ratio of the cross-sectional area to the wetted perimeter), and $S$ is slope of the flow. The typical values of $n$ presents in Table 1.

## 3. Methodology

This study is divided into three main parts. The first part focuses on assessing the performance of height measurements using a GNSS receiver, comparing the heights derived from conventional leveling and GNSS methods. The second part involves determining the slope of the Chao Phraya River basin by collecting elevation data along the riverbanks, from Ayutthaya to Bangkok province. The third part addresses the flow rate (or discharge) of the Chao Phraya River, using Manning's method to back-calculate the Manning's roughness coefficient. The river velocity will be determined once the discharge is known. Finally, the computed discharge will be compared with actual discharge data collected by the Royal Irrigation Department of Thailand. The study workflow illustrates in Figure 3.

*3.1 Study Workflow*

According to Figure 3, the reliability of the heights derived from a GNSS receiver was assessed by setting up seven stations in the mountainous area of Lamphrayaklang Sub-district, Muaklek District, Saraburi Province. The height at each station was determined using the differential leveling method with levels and rods, and was also measured using a GNSS receiver at the same points. The GNSS heights were determined using various techniques, including single positioning, PPP via RTKLib, online PPP, and DGPS by RTKLib. The ellipsoidal heights derived from the GNSS receiver were converted to orthometric heights using the EGM08 model. The height differences calculated from both measurement methods were then compared to evaluate the performance and reliability of orthometric height determination using the GNSS receiver. The slope of the Chao Phraya River basin was determined by placing the GNSS receiver along the riverbank, from Ayutthaya Province to Bangkok. Data were collected at each station for one hour and stored as RINEX files. The coordinates and ellipsoidal heights of each station were determined using several techniques: single positioning, static positioning (rnx2rtkp), RTKLib PPP, and online PPP.

**Table 1**: Manning's roughness coefficient [39]

| Class | Description | Minimum | Normal | Maximum |
|---|---|---|---|---|
| a | Clean, straight, full stage, no rifts or deep pools | 0.025 | 0.030 | 0.033 |
| b | Same as above, but more stone and weeds | 0.030 | 0.035 | 0.040 |
| c | Clean, winding, some pools and shoals | 0.033 | 0.040 | 0.045 |
| d | Same as above, but some weed and stone | 0.035 | 0.045 | 0.050 |
| e | Same as above, lower stages, more ineffective slopes and sections | 0.040 | 0.048 | 0.055 |
| f | Same as "d" with more stone | 0.045 | 0.050 | 0.060 |
| g | Sluggish reaches, weedy, deep pools | 0.050 | 0.070 | 0.080 |
| h | Very weedy reaches, deep pools, or floodways with heavy stand of timber and underbrush | 0.075 | 0.100 | 0.150 |

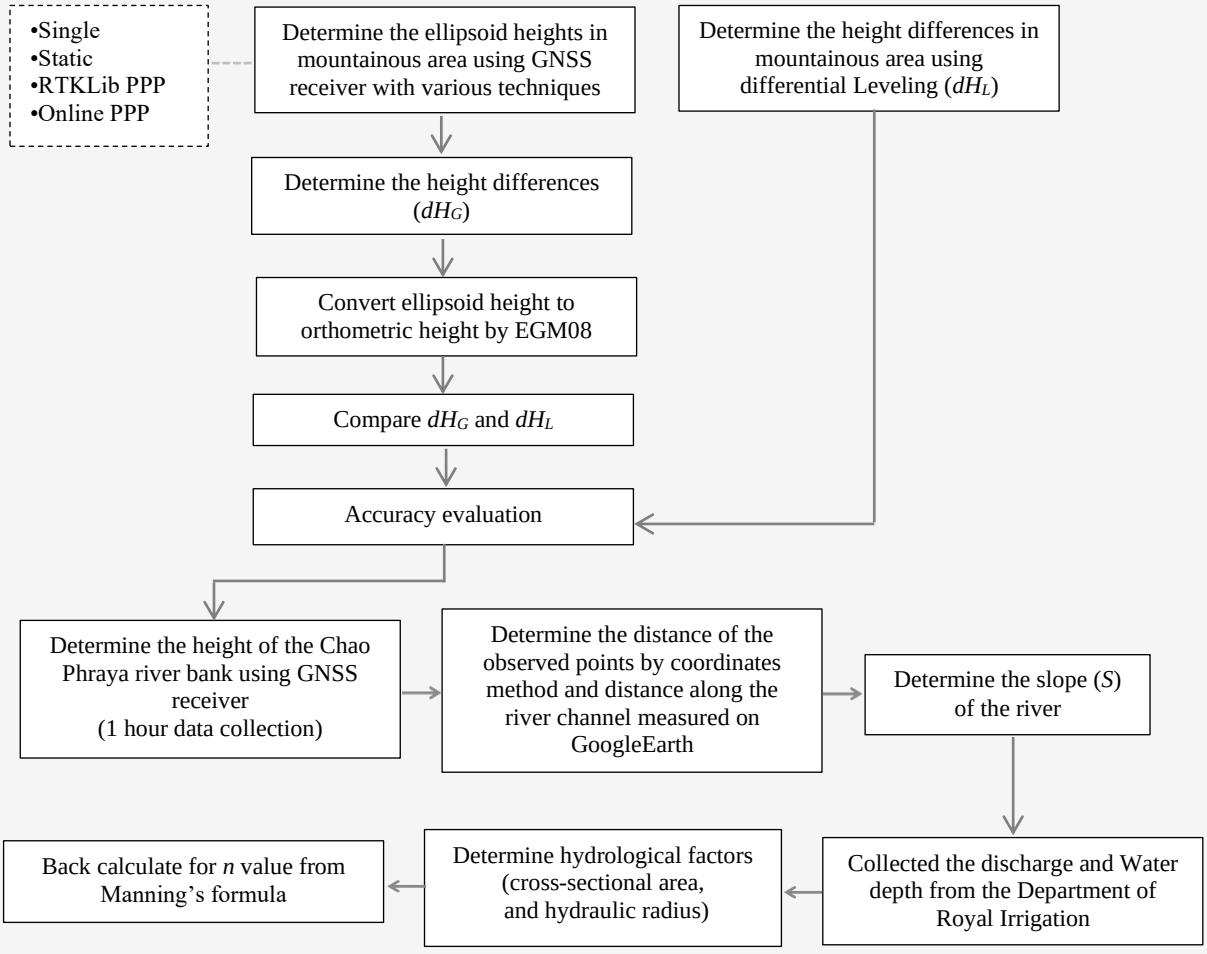


**Figure 3**: The slope of the Chaophraya River and manning coefficient determination workflow

The ellipsoidal heights were then converted to orthometric heights using geoid undulations obtained from the EGM08 geoid model. Finally, the slope of the study area was determined by calculating the relationship between the distances and height differences of the collected points. Manning's roughness coefficient for the river was back-calculated using Manning's formula. The computed discharge was then compared with the real discharge observed by the Department of Royal Irrigation.

*3.2 Data collection*

Data was collected using a "Javad" Sigma GNSS receiver as shown in Figure 4. Each observation station recorded satellite signals for one hour. The stations were located along the Chao Phraya River, from Ayutthaya Province to Bangkok. The collected data were converted into RINEX files using "Netview" software, with a data collection rate of 1 Hz. These RINEX files were then used to compute the coordinates and ellipsoidal heights of the observed stations. A tripod was not required for instrument setup, as the receiver is placed directly on the ground surface. Since the receiver heights are uniform, the terrain height will not be affected by the receiver height, meaning the height of the receiver can be neglected in the height difference calculations. Twelve observation stations were selected in areas that can be accessed without special permission, such as temples and schools. The locations of the observed stations along the Chao Phraya River bank are shown in Figure 5.

*3.3 Post Processing*

The RINEX files were used in the post-processing phase to determine the coordinates and ellipsoidal heights of the observed stations. Various techniques were employed to compute the receiver positions and ellipsoidal heights.


(a)

(b)

**Figure 4**: GNSS measurement (a) field data collection (b) Javad Sigma GNSS receiver

**Table 2:** RTKLib static positioning parameter descriptions [40]

| Parameters | Description |
|---|---|
| *-p* | 0:single, 1:dgps, 2:kinematic, 3:static, 4:moving-base, 5:fixed, 6:ppp-kinematic, 7:ppp-static) |
| *-f* | number of frequencies for relative mode (1:L1,2:L1+L2,3:L1+L2+L5) |
| *-t* | output time in the form of yyyy/mm/dd hh:mm:ss.ss [sssss.ss] |
| *-e* | output x/y/z-ecef position [latitude/longitude/height] |
| *-s* | field separator [' '] |

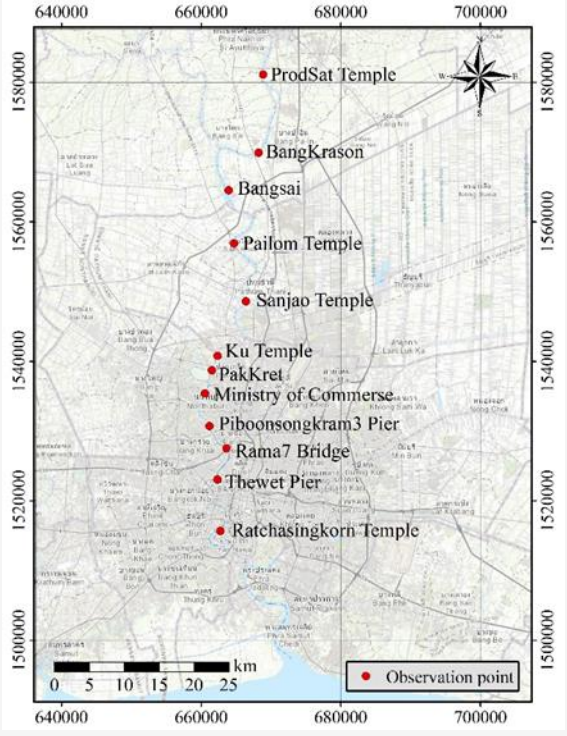


**Figure 5**: Data collection points for slope measurement along the Chao Phraya River

*3.3.1 Static positioning by RTKLib*

The RINEX observation file contained the observations data from the field (rover). In relative mode, the second RINEX observation file contained the observation from the reference (base station) receiver. The base file is downloaded from the Chulalongkorn station (CUSV) reference station, available at: https://cddis.nasa.gov/archive/gnss/data/daily/. Post-processing using the static positioning technique was initiated with the command *>rnx2rtkp -p 3 -f 2 -t -e -s, RINEX_observation_file.o Base_station_file.o_station Navigation_file.n >Output_file.txt*. The detail of the code above shown in Table 2. The coordinates obtained from rnx2rtkp are in the ECEF reference frame, so they must be converted to geographic coordinates.

*3.3.2 Precise Point Positioning*

*3.3.2.1 RTKLib*

Precise Point Positioning (PPP) can be performed using RTKLib with orbit (.sp3)and clock products (.clk) from the IGS. Unlike traditional high-accuracy positioning techniques, PPP does not require a base station to be set up. Instead, it utilizes highly accurate clock and orbit products derived from a global network of reference stations. This allows users to achieve centimeter-level accuracy without being limited by the distance from any particular base station. The orbit and clock products are available on the IGS website and are derived from a global network of continuously operating reference stations maintained by both public and private organizations. RTKPOST in RTKLib software is one of several PPP tools that users can access free of charge [40].

*3.3.2.2 Online precise point positioning using the Natural Resources Canada Canadian Spatial Reference System (CSRS-PPP)*

Precise Point Positioning (PPP) is a GNSS data processing technique that can generate highly precise coordinates. The algorithm behind this technique is somewhat complex, so using online PPP services is a convenient way to obtain more accurate coordinates. For this study, the Canadian Spatial Reference System PPP service (CSRS-PPP) was used to determine the coordinates and ellipsoidal heights of the points in the study area. The CSRS-PPP service is available online at https://webapp.csrs-scrs.nrcan-rncan.gc.ca/geod/tools-outils/ppp.php?locale=en. Generally, more accurate coordinates and ellipsoidal heights can be obtained with longer data files, with 24-hour files being preferable [41] and [42]. However, shorter files can still provide sufficient accuracy, especially when precise satellite orbit and clock data are available.

*3.3.2.3 Online precise point positioning using the GNSS analysis and positioning software (GAPS-PPP)*

Online PPP can also be performed via the website http://gaps.gge.unb.ca/submitbasic.php, which is provided by the University of New Brunswick, Canada [43]. RINEX observation files are submitted through the website for processing, and the results are sent back to the user's specified email. One advantage of this service over CSRS-PPP is that the coordinates of the observed points can be visualized in Google Earth using a .kml file. Additionally, the overall results can be accessed on any web browser.

*3.4 Discharge Data Acquisition*

The flow data and cross-sectional data were downloaded from the Office of Water Management and the Hydrology Department of the Royal Irrigation Department of Thailand at http://hydro-5.rid.go.th/. The data were collected from in November 2024. In this study, observation stations C35, C36, and C37 were selected because they are located in Phranakhon Si Ayutthaya Province (Figure 6), where the study area begins, and the river slope data collection started in this region. The cross-sections and water depths of the three observation stations are depicted in Figure 7.

## 4. Results and Discussion

*4.1 Differential Leveling and GNSS Heights*

Height differences were measured using both differential leveling and GNSS techniques, and the results from both methods were compared. Three observation points with known coordinates and elevations were established. The GNSS receiver was then placed at each point to determine the elevation. The results are presented in Figure 8 and Table 3. Table 3 shows that single point positioning is not suitable for height determination, as the accuracy varies from 4 to 6 meters. The orthometric heights derived from GNSS, computed using Precise Point Positioning (PPP) with both CSRS and GAPS, as well as the Static Positioning (rnx2rtkp) technique, are quite similar to each other. The elevations of the terrain derived from both GNSS techniques are approximately one meter lower than the true orthometric heights. This discrepancy is due to the fact that the orthometric heights in the study area are based on the local geoid at Koh Lak, Prachuapkirikhan Province, Thailand, whereas the GNSS-derived orthometric heights are based on the global geoid (ITRF). Therefore, orthometric heights derived from GNSS receivers are not suitable for determining terrain elevations.

**Table 3**: Differences in orthometric heights between conventional leveling and PPP

| Station No. | Errors = Fixed – Measurement Techniques [m] | | | | |
|---|---|---|---|---|---|
| | Single Pos. | Static (Rnx2rtkp) | CSRS PPP | GAPS PPP | RTKLiB PPP |
| 1 | -6.251 | -0.808 | -0.940 | -0.981 | -1.642 |
| 2 | -4.422 | -0.989 | -1.222 | -1.250 | -0.904 |
| 3 | 4.979 | -0.978 | -1.011 | -0.756 | -0.804 |

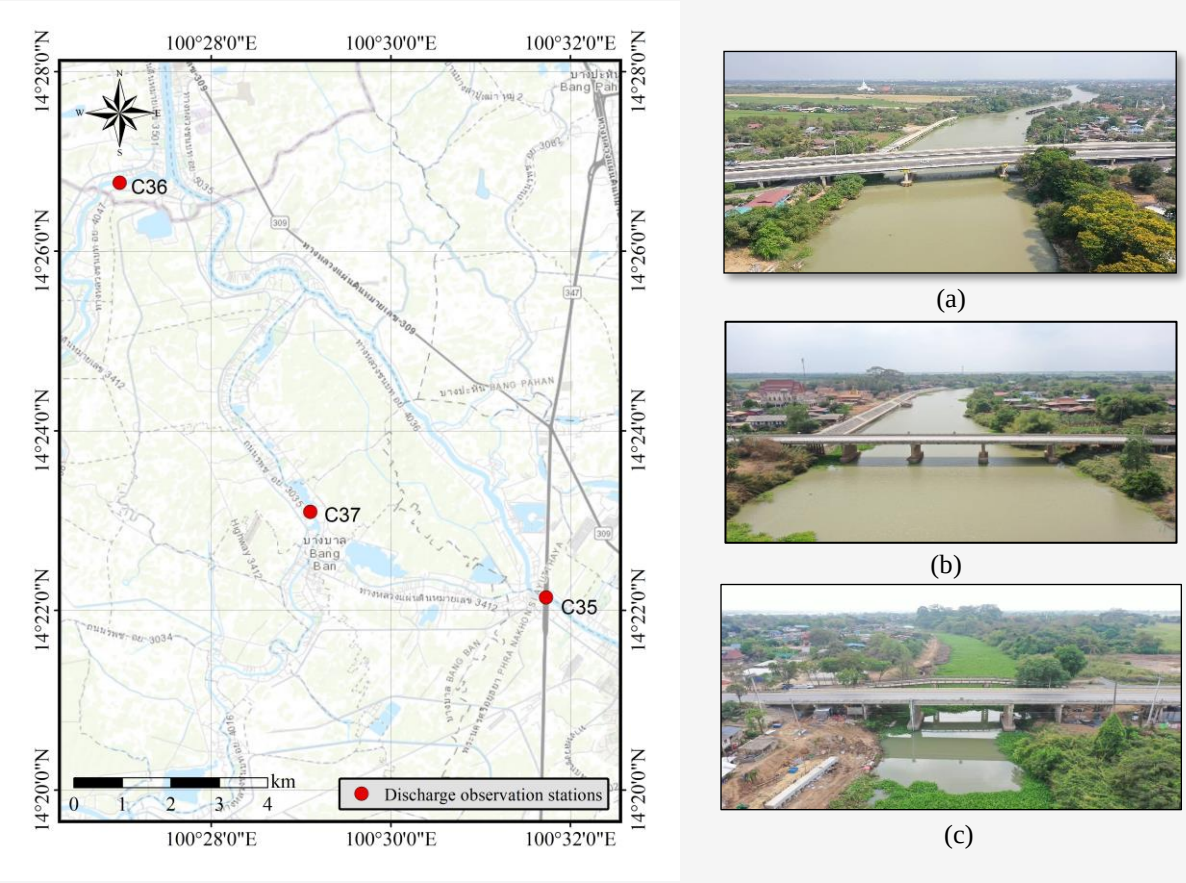


**Figure 6**: Observation stations (a) C35 (b) C36 (c) C37 in Phranakhon Si Ayutthaya province

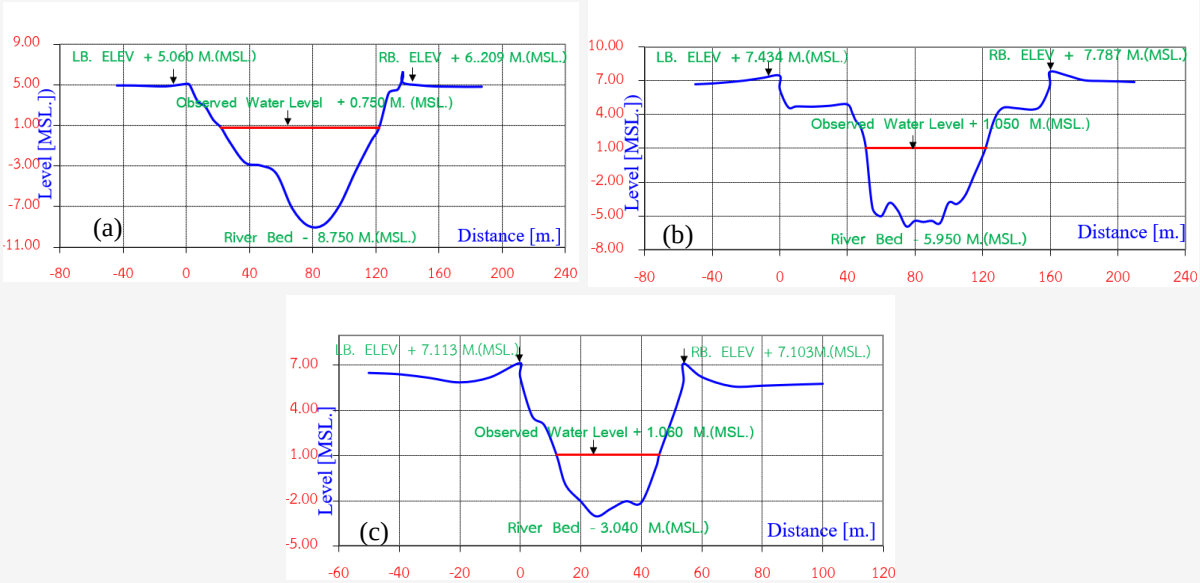


**Figure 7**: Cross-sections of the river at the observation stations (a) C35 (b) C36 (c) C37

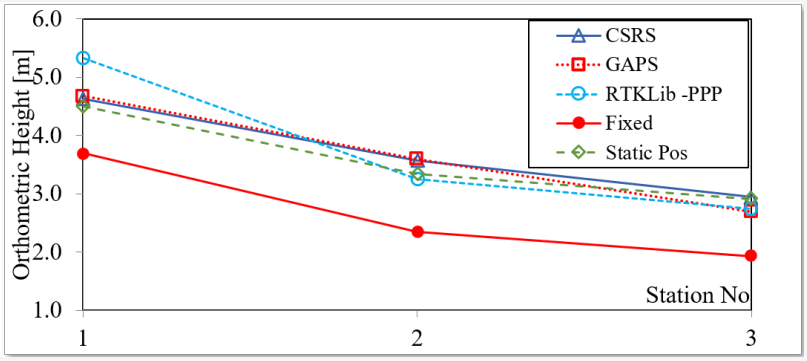


**Figure 8**: Comparison of orthometric heights obtained from conventional leveling and PPP

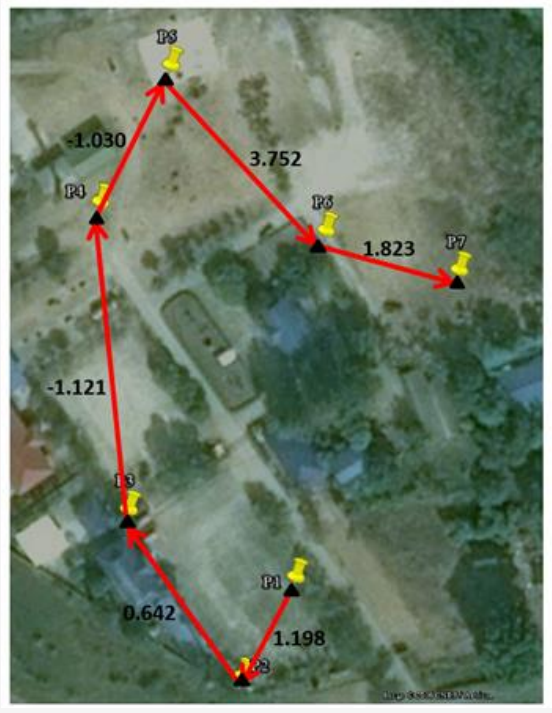


**Figure 9:** Differential leveling test site

*4.2 Assessment of Orthometric Height Derived from Ellipsoid Height*

Based on the previous section, it is clear that the elevations derived from the GNSS receiver are approximately one meter above the actual terrain, raising questions about the feasibility of using GNSS elevation data to determine terrain heights. However, GNSS receivers may still be useful for measuring height differences, making it crucial to validate the height differences derived from GNSS data. Validation was conducted in the mountainous area of Muak Lek District, Saraburi Province, Thailand. Seven stations were established to measure height differences using both conventional leveling and GNSS techniques. The leveling test site and the leveling points present in Figure 9. Table 4 presents the geoid undulations and ellipsoid heights calculated using different computation methods. The orthometric height of each station was determined from Equation 1. The orthometric heights and height differences present in Table 5 and Figure 10, respectively. Since conventional leveling provides the orthometric heights of the terrain and is commonly used to determine height differences, it serves as the reference method for assessing the errors of height differences computed by other techniques. Table 5 and Figure 10 demonstrate that the height differences computed using online PPP, specifically both CSRS and GAPS, are in close agreement with the results from differential leveling.

**Table 4**: Geoid undulation and ellipsoid heights

| Station No. | Geoid undulation [m] | Ellipsoid height [m] | | | | |
|---|---|---|---|---|---|---|
| | | CSRS PPP | GAPS PPP | RTKLib PPP | Static Pos. | Single Pos. |
| 1 | -29.694 | 215.715 | 215.723 | 215.596 | 215.076 | 216.513 |
| 2 | -29.693 | 216.970 | 217.163 | 217.379 | 216.624 | 223.120 |
| 3 | -29.695 | 217.586 | 217.890 | 217.189 | 217.757 | 217.211 |
| 4 | -29.698 | 216.384 | 216.241 | 215.935 | 217.861 | 213.365 |
| 5 | -29.699 | 215.315 | 215.335 | 215.184 | 215.300 | 215.766 |
| 6 | -29.697 | 219.126 | 219.135 | 218.513 | 219.003 | 218.178 |
| 7 | -29.696 | 220.958 | 220.894 | 220.807 | 221.110 | 218.606 |

**Table 5**: Orthometric heights derived from ellipsoid heights and geoid undulations

| Station No. | Orthometric height [m] | | | | |
|---|---|---|---|---|---|
| | CSRS PPP | GAPS PPP | RTKLib PPP | Static Pos. | Single Pos. |
| 1 | 186.022 | 186.029 | 185.902 | 185.383 | 186.820 |
| 2 | 187.277 | 187.470 | 187.686 | 186.931 | 193.427 |
| 3 | 187.891 | 188.195 | 187.494 | 188.062 | 187.516 |
| 4 | 186.686 | 186.543 | 186.237 | 188.163 | 183.667 |
| 5 | 185.616 | 185.636 | 185.485 | 185.601 | 186.067 |
| 6 | 189.429 | 189.439 | 188.817 | 189.306 | 188.481 |
| 7 | 191.263 | 191.199 | 191.112 | 191.415 | 188.911 |

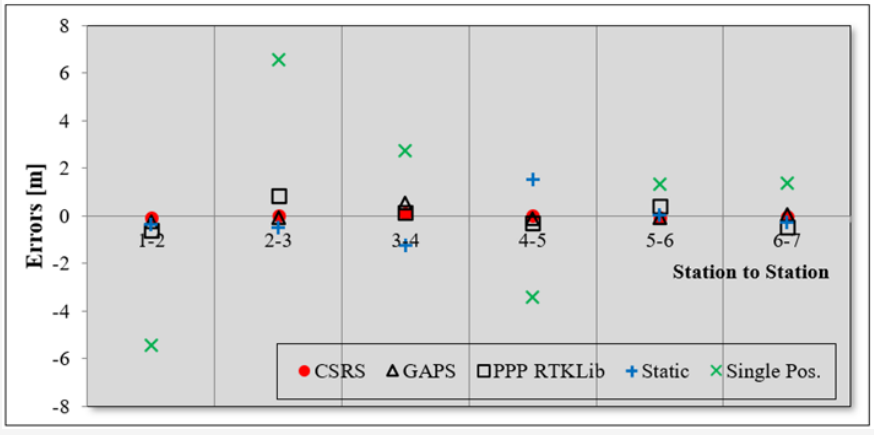


**Figure 10**: Error of height differences between differential leveling and GNSS measurement

The height differences between the points in the test area calculated by the online PPP methods are nearly identical to those derived from differential leveling, whereas other computation techniques exhibit higher errors and more significant deviations from the leveling results. Therefore, height differences derived from the GNSS receiver using online PPP provide the best match with differential leveling data. Figure 11 further illustrates that CSRS-PPP produces height differences that are closer to those obtained from differential leveling compared to GAPS-PPP. As shown in the figure, the circle symbol is positioned near the red cross, which represents the differential leveling result. This suggests that orthometric heights can be accurately computed from the ellipsoid height derived from CSRS-PPP, indicating that GNSS receivers are highly suitable for determining height differences.

Furthermore, Figure 10 clearly shows that the CSRS-PPP technique yields the smallest error in height differences, followed by GAPS-PPP, RTKLib PPP, static (rnx2rtkp), and single positioning, in that order. The error range for height differences computed using CSRS-PPP is between 0.01 and 0.08 meters, while GAPS-PPP shows errors between 0.05 and 0.50 meters.

Based on these results, the CSRS-PPP technique was selected for determining the height of the Chao Phraya River bank to investigate the slope of the river basin. In conclusion, the results of the height difference determinations suggest that GNSS receivers are capable of accurately determining height differences, especially in areas where observation points are widely spaced. The "Online Precise Positioning Point (PPP)" computation method provides the closest approximation of height differences when compared to the conventional leveling technique.

*4.3 Slope of the Chao Phraya River Basin*

Since the online PPP technique provides the most accurate height difference values compared to conventional leveling, the GNSS receiver was employed to determine the terrain heights along the Chao Phraya River for slope analysis in the study area. The measurements were conducted from Ayutthaya Province to Pathum Thani, Nonthaburi, and Bangkok. A total of twelve observation stations were established along the river, with data collected using a Javad GNSS receiver. Each station collected data for approximately one hour, and post-processing was performed using the CSRS-PPP tool at https://webapp.csrs-scrs.nrcan-rncan.gc.ca/geod/tools-outils/ppp.php?locale=en. The distances between the observation points were measured along the river using Google Earth.

Figure 11 illustrates that the slope of the Chao Phraya River is relatively flat, with a slope of 0.00003, approximately corresponding to 1:33,333. The coefficient of determination ($r^2$) is approximately 0.82, indicating that 82% of the variation in elevation can be explained by the distance between observation points. The result is in perfect alignment with the previous study [44]. These results suggest that the Chao Phraya River basin exhibits a north-to-south gradient. Additionally, the results validate the slope measurements obtained using a GNSS receiver, as the river flows from the northern region toward the Gulf of Thailand in the south. The elevation at Nakhon Sawan Province is approximately +20 meters above mean sea level (MSL), while Bangkok's elevation is approximately +2 meters MSL. The distance between these two provinces is approximately 375 kilometers. Based on this data, the approximate slope of the Chao Phraya River basin is 0.000048. However, since the measurement does not follow the river's exact course, some measurement error may be present. Despite this, a slope ratio of 1:33,333 is considered sufficiently accurate for use in hydrological modeling.

*4.4 Manning's Roughness Coefficient Estimation*

The slope of the study area was determined in the previous section, and the Manning coefficients for the Chao Phraya River were calculated using Manning's formula (Equation 2). Data for discharge computations were sourced from the Department of Royal Irrigation of Thailand, available at: http://hydro-5.rid.go.th/. Discharge, cross-sectional area, and river width data were collected and utilized in the back-calculation of Manning's coefficients. Several monitoring stations along the Chao Phraya River begin in Nakhon Sawan Province (station C2), but only three stations in Ayutthaya Province (C35, C36, and C37), as shown in Figure 6, were considered for this analysis. These stations were selected due to the availability of slope measurements and river cross-sectional data in this region.

Manning's formula, presented in Equation 2, allows for the calculation of discharge in an open channel. Given known values for discharge, width, and cross-sectional area of the river, the Manning roughness coefficient can be determined. The Manning coefficients were back-calculated from the data provided in Table 6.

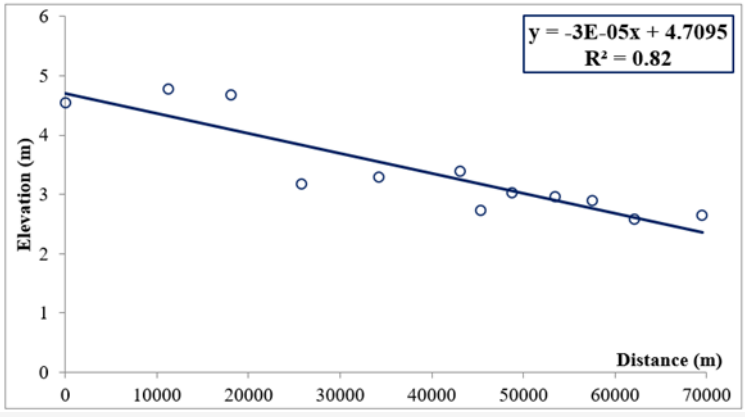


**Figure 11**: Determination of the slope of the Chao Phraya River

**Table 6**: The back-calculation of Manning's roughness coefficients

| Station | C35 | C36 | C37 |
|---|---|---|---|
| Cross sectional area; *A* (sq.m) | 516.445 | 252.43 | 102.5 |
| Wet perimeter; *P* (m) | 107.09 | 75.13 | 35.24 |
| Hydraulic radius; *R* (m) | 4.82 | 3.36 | 2.91 |
| Discharge; *Q* (cms) | 228 | 80.54 | 25.48 |
| Slope; *S* | | 1:33333 | |
| Manning's roughness coefficients; *n* | 0.035 | 0.039 | 0.045 |

**Table 7**: Hydrological parameters for discharge and flow velocity

| Station | Cross sectional area; A [sq.m.] | Hydraulic radius; R [m.] | Discharge [cms] | Velocity [m/s] |
|---|---|---|---|---|
| C35 | $A$=128.64$y$ + 361.71 | $R$=4.5895$y$ + 0.4182 | $Q$=19.521$y^2$ + 192.61$y$ + 47.507 | $V$=0.233$y$ + 0.355 |
| C36 | $A$=76.701$y$ + 259.96 | $R$=4.1499$y$ + 1.604 | $Q$=6.122$y^2$ + 67.342$y$ + 37.94 | $V$=0.160$y$ + 0.136 |
| C37 | $A$=37.976$y$ + 74.954 | $R$=7.4503$y$ + 0.7885 | $Q$=3.201$y^2$ + 22.179$y$ + 4.6333 | $V$=0.163$y$ + 0.076 |

The manning's roughness coefficients at stations C35, C36, and C37 are 0.035, 0.039, and 0.045, respectively. The average value of the coefficient is 0.040. The manning's coefficient at each station are not identical because of several factors that influence flow resistance. These include the composition of the riverbed, such as the presence of sand, gravel, or rocks; the type and density of vegetation, which can increase roughness, and the shape and size of the channel, with meanders and irregularities adding resistance [45] and [46]. Additionally, features like bank and bed obstructions, including boulders or fallen trees, contribute to variations in roughness. The coefficient is highest at station C37, likely due to the presence of weeds and water hyacinth covering the riverbank at this location [47] (see Figure 6(c)). The Manning's roughness coefficients derived from this study can be informative and useful to be used in hydrogogical model as SWAT and HEC-RAS models [48].

*4.5 Verification of the Manning's Roughness Coefficient*

Since the Manning's *n* values were derived from flow data, their accuracy must be verified to ensure they are suitable for discharge computations in the Chao Phraya River. Essential parameters for discharge calculation include the cross-sectional area and the wetted perimeter of the channel. Typically, only the water level above mean sea level (MSL) is measured at each observation station, and the river's irregular shape, unlike that of man-made concrete canals, makes it challenging to directly calculate the cross-sectional area and wetted perimeter. As a result, discharge calculations cannot be accurately performed without these measurements.

Discharge is usually determined using a rating curve, which represents the relationship between water level and discharge. The velocity of water flow can be calculated by dividing the discharge by the cross-sectional area of the channel, enabling the plotting of the relationship between water level and river flow velocity. As per Equation 2, the hydraulic radius can be back-calculated, given that the Manning's roughness coefficient, river slope, and cross-sectional area of the channel are known.

Since cross-sectional area data are typically unavailable, and only water levels are observed, Manning's formula cannot be applied without knowledge of the river's cross-sectional area. Therefore, it is essential to investigate and establish the relationship between water level and cross-sectional area. Figure 12 illustrates this relationship, while Figure 13 shows the correlation between water level and hydraulic radius at stations C35, C36, and C37. The hydrological parameters required for determining cross-sectional area ($A$), hydraulic radius ($R$), discharge ($Q$) and flow velocity ($V$) can be derived from the river depth ($y$), as detailed in Table 7.

*4.6 Validation of the Models*

To validate the model parameters derived in the previous sections, the discharges of the Chao Phraya River at stations C35, C36, and C37 on other days were computed using the correlations presented in Figures 12 and 13, along with the Manning's *n* and slope values determined in Sections 4.3 and 4.4. In this case, discharges were easily calculated directly from the established relationships, eliminating the need for the complex formula with multiple parameters, as shown in Equation 2. A comparison between the actual discharges, provided by the Department of Royal Irrigation, and the modeled discharges is presented in Figure 14. The comparison between actual and computed discharges reveals that at station C35, the discharge differences range from 0.04 to 59.83 cubic meters per second (cms), with a mean difference of 40.67 cms.

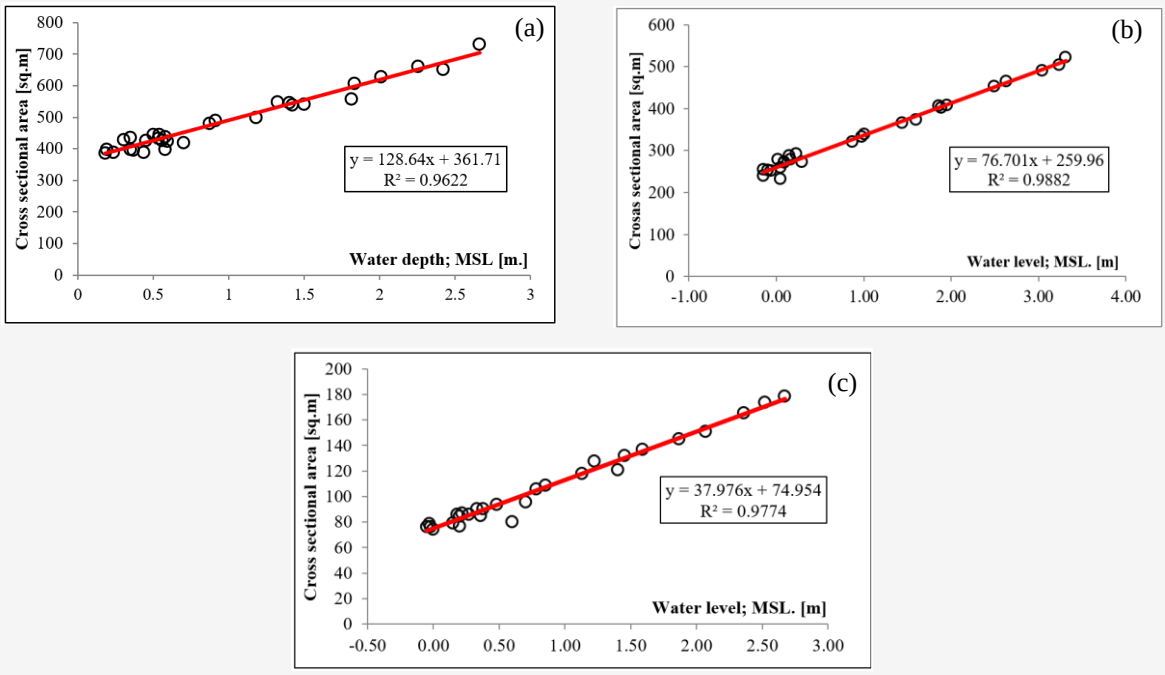


**Figure 12**: Correlation between river depth and cross sectional area: (a) C35 (b) C36 (c) C37

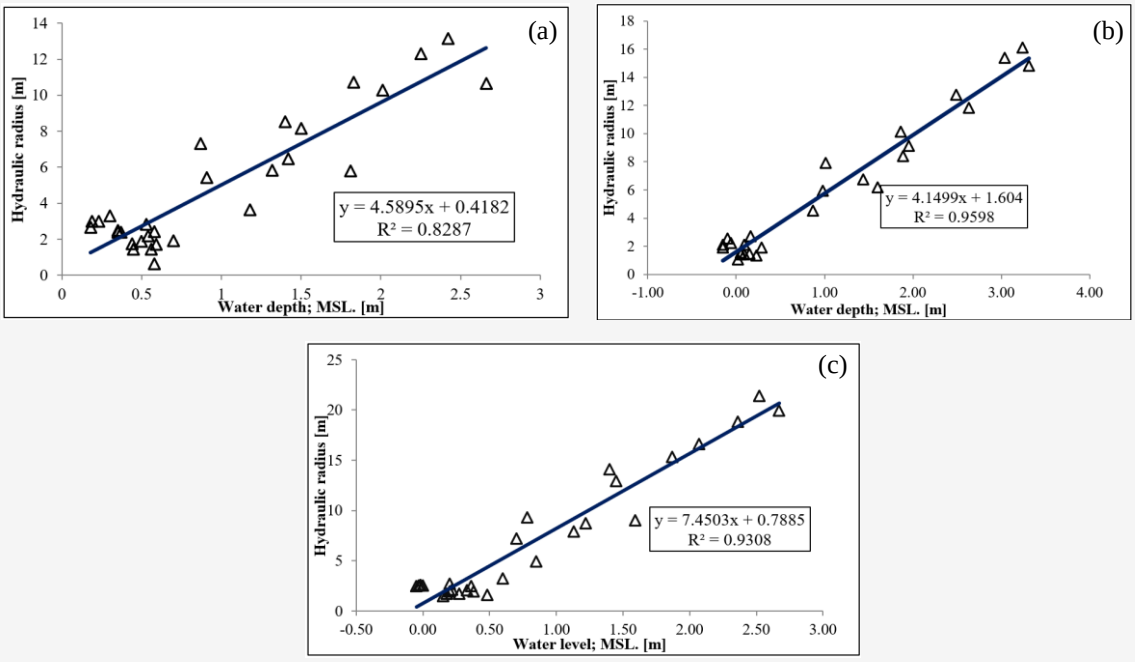


**Figure 13**: Correlation between river depth and hydraulic radius (a) C35 (b) C36 (c) C37

As shown in Figure 14, the discrepancies between actual and computed discharges are notably higher during the summer and winter seasons, while the differences are smaller during the rainy season (August to November). Average discharges during the summer (March to July) and winter (November to April) are approximately 200-250 cms, whereas the highest discharge occurs in the rainy season, with a peak of 700 cms in August. The larger discrepancies between modeled and actual discharges in the summer and winter can be attributed to variations in the roughness between the water and the riverbank.

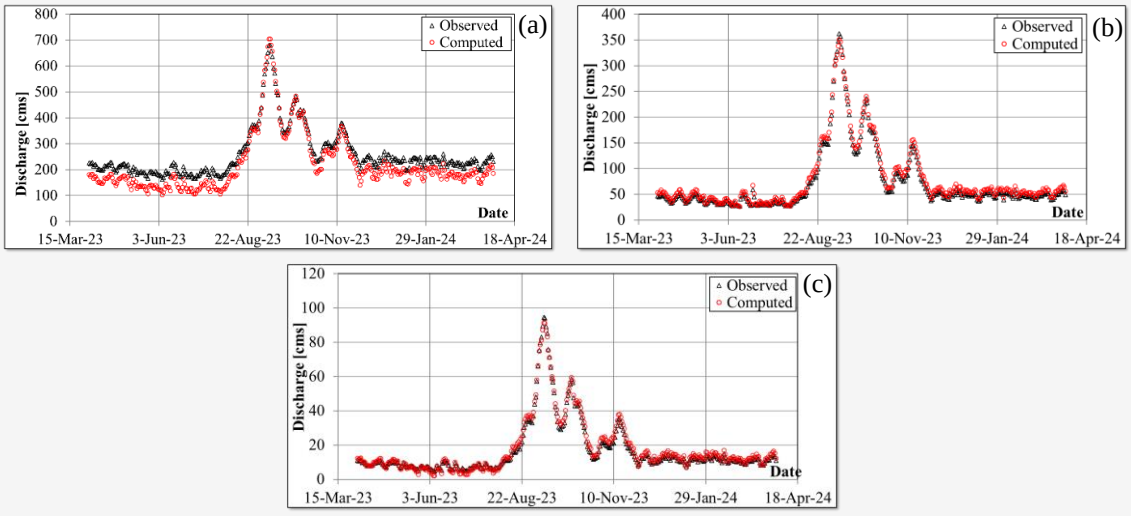


**Figure 14**: Comparison of actual and modeled discharge values (a) C35 (b) C36 (c) C37

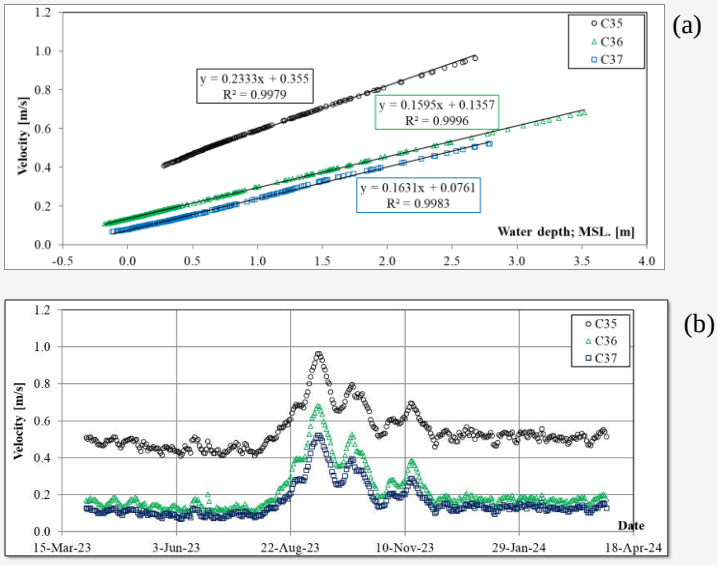


**Figure 15**: Velocity of river flow: (a) correlation between river depth and velocity (b) velocity modeling

Consequently, the Manning's n values derived from the model may not remain constant throughout the year. At station C35, the river width is the widest compared to stations C36 and C37, which may contribute to the higher differences observed. However, the modeled discharge aligns well with actual discharge during the rainy season, indicating that the derived parameters and the model are reliable for estimating discharges during this period, which is crucial for flood assessments. At stations C36 and C37, the comparison between computed and actual discharges shows smaller discrepancies, with differences ranging from 0.02 to 11.76 cms at C36 and 0.03 to 3.17 cms at C37. The river widths at these stations are smaller than at C35, and thus the Manning's n values are less affected by variations in water depth. Therefore, the models for stations C36 and C37 are more suitable for estimating discharge throughout the year.

*4.7 Velocity of the River Flow*

The flow velocity can be easily calculated by dividing the discharge by the river's cross-sectional area. Since the cross-sectional area is proportional to the river depth, as depicted in Figure 12, the velocity at each station can be estimated based on the river depth, as shown in Figure 15. The velocities computed using Manning's formula and those derived from the relationship in Figure 15(a) show a consistent difference of approximately 0.01 m/s at each observed station.

This indicates that the relation in Figure 15(a) can reliably predict river flow velocities. This is particularly valuable for determining evacuation times during periods of high water or flooding events. Figure 15(b) demonstrates that the velocity of the Chao Phraya River at station C35 is approximately 0.4 m/s (34.56 km/day) during the summer and 0.5 m/s (43.2 km/day) in winter. However, during the rainy season (August to November), the velocity fluctuates in response to changes in discharge. At stations C36 and C37, the velocities are similar, with values of about 0.1 m/s (8.64 km/day) in summer and 0.2 m/s (17.28 km/day) in winter, with variations also occurring during the rainy season. As shown in Figure 15(b), the velocity at station C35 is approximately three times faster than at station C36 and five times faster than at station C37.

## 5. Conclusions

This study successfully determined the slope of the Chao Phraya River and Manning's roughness coefficients using GNSS-based Precise Point Positioning (PPP) techniques. The results confirm that GNSS measurements, particularly those processed through online PPP services such as CSRS-PPP, provide highly accurate height differences suitable for slope calculations. The computed slope of 0.00003 (1:33,333) aligns with the expected topographical gradient from Nakhon Sawan to Bangkok and previous study. Manning's roughness coefficients, essential for flow modeling, were back-calculated using observed discharge data and Manning's equation. The derived coefficients varied from 0.035 to 0.045, reflecting differences in riverbed characteristics, vegetation, and channel geometry. The highest roughness coefficient was observed at station C37, likely due to extensive vegetation along the riverbanks. Validation of the roughness coefficients using observed discharge data indicated that seasonal variations significantly influence flow resistance, with higher discrepancies occurring during dry seasons due to changes in channel morphology and sediment deposition.

Additionally, the study established empirical relationships between river depth and hydrological parameters such as cross-sectional area, hydraulic radius, and discharge. These relationships allow for more efficient estimation of flow characteristics based on observed water levels, reducing dependency on direct discharge measurements. The velocity modeling further demonstrated the seasonal variability in river flow rates, highlighting the importance of accurate roughness coefficient estimation for flood forecasting. Despite the successful implementation of GNSS-based methodologies, some limitations were identified. The accuracy of orthometric height conversion depends on geoid models, and localized geoid variations may introduce minor errors. Moreover, the study's focus on a limited number of observation stations may not fully capture the spatial variability in riverbed conditions. Future research should expand the dataset to include more stations and integrate real-time monitoring techniques for continuous slope and flow assessments.

## 6. Recommendation

To enhance flood prediction and management in the Chao Phraya River basin, this study recommends integrating real-time GNSS monitoring for improved slope and elevation data, refining geoid models for greater accuracy, and expanding observation stations to better capture variations in Manning's roughness coefficients. The incorporation of remote sensing data, such as LiDAR and satellite imagery, can enhance terrain assessments. Seasonal calibration of roughness coefficients is necessary to account for changes in vegetation and sediment deposition. Additionally, developing advanced predictive models that integrate GNSS-based slope measurements and real-time discharge data will improve flood preparedness. Public awareness and policy implementation should also be prioritized through early warning systems and comprehensive flood risk mapping. Implementing these strategies will strengthen Thailand's flood resilience, minimizing the impact of future flood events on communities and infrastructure.

## References


[1] Gale, L., E. and Saunders, A., M., (2013). The 2011 Thailand Flood: Climate Causes and Return Periods. *Weather*, Vol. 68(9). 223-237. https://doi.org/10.1002/wea.2133.

[2] NASA Earth Observatory, (2011). Flooding in Thailand. [Online]. Available: https://earthobservatory.nasa.gov/images/76683/flooding-in-thailand. [Accessed: Nov. 19, 2024].

[3] Promchote, P., Simon Wang, Y. S. and Johnson, G. P., (2016). The 2011 Great Flood in Thailand: Climate Diagnostics and Implications from Climate Change. *Journal of Climate*, Vol. 29(1), 367-379. https://doi.org/10.1175/JCLI-D-15-0310.1.

[4] Marks, D., (2019). Assembling the 2011 Thailand Floods: Protecting Farmers and Inundating High-Value Industrial Estates in A Fragmented Hydro-Social Territory. *Political Geography*, Vol. 68, 66-76. https://doi.org/10.1016/j.polgeo.2018.10.002.

[5] Loc, H. H., Emadzadeh, A., Park, E., Nontikansak, P. and Deo, R. C., (2023). The Great 2011 Thailand Flood Disaster Revisited: Could It Have Been Mitigated by Different Dam Operations Based on Better Weather Forecasts?. *Environmental Research*, Vol. 216 ttps://doi.org/10.1016/j.envres.2022.114493.

[6] Khunwishit, S., Choosuk, C. and Webb, G., (2018). Flood Resilience Building in Thailand: Assessing Progress and the Effect of Leadership. *International Journal of Disaster Risk Science*, Vol. 9, 44–54. https://doi.org/10.1007/s13753-018-0162-0.

[7] Kumne, W. and Samanta, S., (2023). Geospatial Mapping of Inland Flood Susceptibility Based on Multi-Criteria Analysis - A Case Study in the Final Flow of Busu River Basin, Papua New Guinea. *International Journal of Geoinformatics,* Vol. 19(6), 31–48. https://doi.org/10.52939/ijg.v19i6.2693.

[8] Zulhisham, N. and Md Sadek, E., (2023). Employing the Flash Flood Potential Index (FFPI) with Physical Environmental Factors in Baling, Kedah through GIS Analysis. *International Journal of Geoinformatics*, Vol 19(5), 19–29. https://doi.org/10.52939/ijg.v19i5.2653.

[9] Mohd Rasu, M., Suhandri, H., Khalifa, N., Abdul Rasam, A. and Hamid, A., (2023). Evaluation of Flood Risk Map Development through GIS-Based Multi-Criteria Decision Analysis in Maran District, Pahang - Malaysia. *International Journal of Geoinformatics*, Vol. 19(10), 1–16. https://doi.org/10.52939/ijg.v19i9.2873.

[10] Nguyen, D., Chou, T., Hoang, T. and Chen, M., (2023). Flood Susceptibility Mapping Using Machine Learning Algorithms: A Case Study in Huong Khe District, Ha Tinh Province, Vietnam. *International Journal of Geoinformatics*, Vol. 19(7), 1-15. https://doi.org/10.52939/ijg.v19i7.2739.

[11] Wanthong, P., (2016). *Determination of Land Slope and Computation of the Flow Rate of the Chao Phraya River using GNSS*. Master Thesis. Remote Sensing and GIS FoS. Asian Institute of Technology.

[12] Li, B., Lou, L. and Shen, Y., (2015). GNSS Elevation-Dependent Stochastic Modeling and its Impacts on the Statistic Testing. *Journal of Surveying Engineering*, Vol. 14(2). https://doi.org/10.1061/(ASCE)SU.1943-5428.0000156.

[13] Szot, T. and Sontowski, M., (2024). Evaluation of Elevation Parameter Determination by Global Navigation Satellite Systems' Sports Receivers: A Preliminary Study. *Baltic Journal of Health and Physical Activity*, Vol. 16(2). https://doi.org/10.29359/BJHPA.16.2.04.

[14] Aziz, M., Pa'suya, M., Talib, N., Din, A., Hashim, S. and Ramli, M., (2023). Vertical Accuracy Assessment of Improvised Global Digital Elevation Models (MERIT, NASADEM, EarthEnv) Using GNSS and Airborne IFSAR DEM. *International Journal of Geoinformatics*, Vol. 19(12), 65-82. https://doi.org/10.52939/ijg.v19i12.2979.

[15] Tran, N., Nguyen, T., Nguyen, T., Doan, T., Nguyen, T. and Dao, T., (2024). Simulation of Water Quality in Bung Binh Thien Lake, A Giang Province, Vietnam, Using the Delft3D Model. *International Journal of Geoinformatics*, Vol. 20(8), 56-71. https://doi.org/10.52939/ijg.v20i8.3455.

[16] Ngo, A., Grivel, S., Nguyen, T. and Nguyen, T., (2023). Impact Assessment of Land Use and Land Cover Change on the Runoff Changes on the Historical Flood Events in the Laigiang River Basin of the South Central Coast Vietnam. *International Journal of Geoinformatics*, Vol. 19(10), 51-63. https://doi.org/10.52939/ijg.v19i9.2881.

[17] Jular, P., (2017). Thailand: The 2011 Floods in The Lower Chao Phraya River Basin in Bangkok Metropolis. [Online]. Available: https://iwrmactionhub.org/case-study/thailand-2011-floods-lower-chao-phraya-river-basin-bangkok-metropolis. [Accessed: Nov. 25, 2024].

[18] The Nation. (2024). Residents of 11 Provinces Along Banks of Chao Phraya Warned of Rising Water. [Online]. Available: https://www.nationthailand.com/news/general/40040883. [Accessed: Dec. 15, 2024].

[19] Dalai, K., T., Nishimura, K. and Nozaki, Y., (2005). Geochemistry of Molybdenum in the Chao Phraya River Estuary, Thailand: Role of Suboxic Diagenesis and Porewater Transport. *Chemical Geology*, Vol. 218(3-4), 189-202. https://doi.org/10.1016/j.chemgeo.2005.01.002

[20] Future Earth Coasts, IPO. (2000). R&S 14. Estuarine Systems of the South China Sea Region: Carbon, Nitrogen and Phosphorus Fluxes. https://doi.org/10.13140/RG.2.1.4708.5283.

[21] Sayama, T., Tatebe, Y., Iwami, Y. and Tanaka, S., (2015). Hydrologic Sensitivity of Flood Runoff and Inundation: 2011 Thailand Floods in the Chao Phraya River Basin. *Natural Hazards and Earth System Sciences*, Vol. 15, 1617-1630. https://doi.org/10.5194/nhess-15-1617-2015, 2015.

[22] Supharatid, S., (2016). Skill of Precipitation Projection in the Chao Phraya River Basin by Multi-Model Ensemble CMIP3-CMIP5. *Weather and Climate Extremes*, Vol. 12, 1-14. https://doi.org/10.1016/j.wace.2016.03.001.

[23] Rangsiwanichpong, P., Kazama, S. and Ekkawatpanit, C., (2016). Assessment of Flood and Drought Using Ocean Indices in the Chao Phraya River Basin, Thailand. *The 7th International Conference on Water Resources and Environment Research; ICWRER2016*. Kyoto, Japan.

[24] Cermakova, K., (2019). Flood Risk Analysis in the Chao Phraya River Basin in Thailand. Master Thesis. Fakulta stavební Katedra hydrauliky a hydrologie. České Vysoké Učení Technické V Praze.

[25] Wanthong, P., (2014). *Height Systems Calculations at Swabian Alb Test Area.* Master Thesis. University of Stuttgart. [Online]. Available: https://elib.uni-stuttgart.de/handle/11682/3967. [Accessed: Jan. 25, 2024].

[26] Nilipovskiy, V., Elshewy, M. and Hamdy, A., (2022). A Local Geoid for Egypt's Mediterranean Coast: A Model Based on Artificial Neural Networks. *International Journal of Geoinformatics*, Vol. 18(3), 1-11. https://doi.org/10.52939/ijg.v18i3.2193.

[27] Kamto, P., G., Adiang, C., M., Nguiya, S., Kamguia, J. and Yap, L., (2020). Refinement of Bouguer Anomalies Derived from the EGM2008 Model, Impact on Gravimetric Signatures in Mountainous Region: Case of Cameroon Volcanic Line, Central Africa. *Earth and Planet Physics*, Vol. 4(6), 639-650. https://doi.org/10.26464/epp2020065.

[28] Pavlis, N., K., Holmes, A., S., Kenyon, S., C. and Factor, J., (2012). The Development and Evaluation of the Earth Gravitational Model 2008 (EGM2008). *Journal of Geophysical Research Atmospheres*. Vol 118(5). https://doi.org/10.1029/2011JB008916.

[29] Zafirah, Z., Sulaiman, S., Natnan, S., Idris, A. and Satirapod, C., (2023). Quality Assessment of Various CHC NAV GNSS Receiver Models. *International Journal of Geoinformatics*, Vol. 19(5), 31-42. https://doi.org/10.52939/ijg.v19i5.2655.

[30] Charoenkalunyuta, T., Satirapod, C., Charoenyot, R. and Thongtan, T., (2023). Geometric and Statistical Assessments on Horizontal Positioning Accuracy in Relation with GNSS CORS Triangulations of NRTK Positioning Services in Thailand. *International Journal of Geoinformatics*, Vol. 19(2), 1–9. https://doi.org/10.52939/ijg.v19i2.2559.

[31] Kandil, I., Awad, A. and El-Mewafi, M., (2023). Role of Multi-Constellation GNSS in the Mitigation of the Observation Errors and the Enhancement of the Positioning Accuracy. *International Journal of Geoinformatics*, Vol. 19(4), 25-35. https://doi.org/10.52939/ijg.v19i4.2631.

[32] Pa'suya, F., Talib, N., Narashid, R., Ahmad Fauzi, A., Amri Mohd, F. and Abdullah, M., (2022). Quality Assessment of TanDEM-X DEM 12m Using GNSS-RTK and Airborne IFSAR DEM: A Case Study of Tuba Island, Langkawi. *International Journal of Geoinformatics*, Vol. 18(5), 87-103. https://doi.org/10.52939/ijg.v18i5.2389.

[33] Thammaboribal, P., Tripathi, N. and Lipiloet, S., (2024). Pre-Seismic Signature Detection using Diurnal GPS-TEC and Kriging Interpolation Maps (ASK-VTEC Technique): 11 May 2011, M9.0 Tohoku Earthquake Case Study. *International Journal of Geoinformatics*, Vol. 20(11). 148-161. https://doi.org/10.52939/ijg.v20i11.3715.

[34] Thammaboribal, P., Tripathi, N., K., Ninsawat, S. and Pal, I., (2022). Earthquake Precursory Detection Using Diurnal GPS-TEC and Kriging Interpolation Maps: 12 May 2008, Mw7.9 Wenchuan Case Study. *MethodsX*. Vol. 9. https://doi.org/10.1016/j.mex.2022.101617.

[35] Elshewy, M., Hamdy, A. and Elsheshtawy, A., (2020). Improving the Accuracy of GNSS Data in the Absolute Point Positioning Based on Linear Relational Model. *International Journal of Geoinformatics*, Vol. 16(4), 51-57. https://journals.sfu.ca/ijg/index.php/journal/article/view/1797.

[36] Mustafin, M., Nasrullah, M. and Abboud, M., (2024). A Comparative Analysis of GNSS Processing Services for Static Measurements: Evaluating Accuracy and Stability at Different Observation Periods. *International Journal of Geoinformatics*, Vol. 20(9), 112–121. https://doi.org/10.52939/ijg.v20i9.3553.

[37] Uaratanawong, V., Tangvijitjankarn, K. and Satirapod, C., (2024). Performance of a Low-Cost GNSS Receiver Using MADOCA Corrections with Precise Point Positioning (PPP) Mode in Thailand. *International Journal of Geoinformatics*, Vol. 20(5), 69-78. https://doi.org/10.52939/ijg.v20i5.3233.

[38] Sabah, S. and Bachir, A. (2023). Manning's Roughness Coefficient in a Truncated Triangular Open-Channel Flow Section. *Water Practice & Technology*, Vol. 18(4). https://doi.org/10.2166/wpt.2023.044.

[39] Chow, V. T., (1959). *Open-Channel Hydraulics.* New York, McGraw-Hill.

[40] RTKLib, (2013). *RTKLIB ver. 2.4.2 Manual*. [Online]. Available: https://www.rtklib.com/prog/manual_2.4.2.pdf. [Accessed: Dec. 25, 2024].

[41] Pierre Tetreault, P., Kouba, J., Heroux, P. and Legree, P. (2005). CSRS-PPP: AN Internet Service for GPS User Access to the Canadian Spatial Reference Frame. Geomatica, Vol. 59(1), 17-28. https://doi.org/10.5623/geomat-2005-0004.

[42] Klatt, C. and Johnson, P., (2017). A Survey of Surveys: The Canadian Spatial Reference System Precise Point Positioning Service. *Geomatica*, Vol 71(1), 27-36. https://doi.org/10.5623/cig2017-103.

[43] Leandro, F., R., Santos, M. and Langley, R. B., (2007). GAPS: The GPS Analysis and Positioning Software - A Brief Overview. *ION GNSS 20th International Technical Meeting of the Satellite Division*. Forth Worth, Texas.

[44] Chaiwongsaen, N., Parisa, N. and Montri, C., (2019). Morphological Changes of the Lower Ping and Chao Phraya Rivers, North and Central Thailand: Flood and Coastal Equilibrium Analyses. *Open Geosciences*, Vol. 11(1), 152-171. https://doi.org/10.1515/geo-2019-0013.

[45] Ngo, A., Grivel, S., Nguyen, T. and Nguyen, T., (2023). Impact Assessment of Land Use and Land Cover Change on the Runoff Changes on the Historical Flood Events in the Laigiang River Basin of the South Central Coast Vietnam. *International Journal of Geoinformatics*, Vol. 19(10), 51-63. https://doi.org/10.52939/ijg.v19i9.2881.

[46] Tran, N., Nguyen, T., Nguyen, T., Doan, T., Nguyen, T. and Dao, T., (2024). Simulation of Water Quality in Bung Binh Thien Lake, A Giang Province, Vietnam, Using the Delft3D Model. *International Journal of Geoinformatics*, Vol. 20(8), 56-71. https://doi.org/10.52939/ijg.v20i8.3455.

[47] Chuenchooklin, S., Mekprugsawong, P. and Chidchob, P., (2007). The River Analysis Simulation Model for the Planning of Retention Area and Diversion Channel for Flood Reduction in the Lower Yom's River Basin, Thailand. *4th INWEPF Steering Meeting and Symposium*. July 5-7, 2007. Bangkok.

[48] Alshammari, E., Abdul Rahman, A., Ranis, R., Abu Seri, N. and Ahmad, F., (2024). Investigation of Runoff and Flooding in Urban Areas based on Hydrology Models: A Literature Review. *International Journal of Geoinformatics*, Vol. 20(1), 99–119. https://doi.org/10.52939/ijg.v20i1.3033.